Detection of breast cancer with ultrasound tomography: First results with the Computed Ultrasound Risk Evaluation (CURE) prototype

Nebojsa Duric[a] and Peter Littrup
Karmanos Cancer Institute, 110 East Warren, Hudson-Webber Cancer Research Center, Room 4246, Detroit, Michigan 48201

Lou Poulo
Analogic Corporation, Peabody Massachusetts 01960

Alex Babkin
Groupvelocity, LLC, Albuquerque New Mexico 87131

Roman Pevzner
DECO Geophysical, Moscow, Russia

Earle Holsapple, Olsi Rama, and Carri Glide
Karmanos Cancer Institute, 110 East Warren, Hudson-Webber Cancer Research Center, Room 4246, Detroit, Michigan 48201

(Received 28 September 2006; revised 18 December 2006; accepted for publication 18 December 2006; published 30 January 2007)

Although mammography is the gold standard for breast imaging, its limitations result in a high rate of biopsies of benign lesions and a significant false negative rate for women with dense breasts. In response to this imaging performance gap we have been developing a clinical breast imaging methodology based on the principles of ultrasound tomography. The Computed Ultrasound Risk Evaluation (CURE) system has been designed with the clinical goals of whole breast, operator-independent imaging, and differentiation of breast masses. This paper describes the first clinical prototype, summarizes our initial image reconstruction techniques, and presents phantom and preliminary *in vivo* results. In an initial assessment of its *in vivo* performance, we have examined 50 women with the CURE prototype and obtained the following results. (1) Tomographic imaging of breast architecture is demonstrated in both CURE modes of reflection and transmission imaging. (2) In-plane spatial resolution of 0.5 mm in reflection and 4 mm in transmission is achieved. (3) Masses >15 mm in size are routinely detected. (4) Reflection, sound speed, and attenuation imaging of breast masses are demonstrated. These initial results indicate that operator-independent, whole-breast imaging and the detection of breast masses are feasible. Future studies will focus on improved detection and differentiation of masses in support of our long-term goal of increasing the specificity of breast exams, thereby reducing the number of biopsies of benign masses. © *2007 American Association of Physicists in Medicine*. [DOI: 10.1118/1.2432161]

I. INTRODUCTION

Mammography screening has been shown to reduce the mortality rate in multiple screening trials.[1] However, diagnostic mammography generates many abnormal findings not related to cancer, leading to additional, costly imaging procedures and biopsies.[2] *Specificity* is the most important benefit-cost factor impacting early detection testing.[3–5] A mammogram finding is not specific because its two main diagnostic criteria, the identification of calcium deposits and masses, are also seen with noncancerous breast changes. Consequently the false positive rate associated with diagnosing breast masses can be as high as 80%. The differentiation of benign from malignant tissue in mammogram findings is further hampered by the added density of normal breast parenchyma in younger women. Thus, for young women and women with dense breasts the false negative rate can be as high as 50%, indicating lower *sensitivity* in these cases. For these reasons, mammography is, therefore, generally complemented by ultrasound (US) which helps differentiate cysts from solid masses and has become the dominant mode for guiding needle biopsy. Recent studies have demonstrated the effectiveness of US imaging in detecting breast cancer,[6] particularly for women with dense breasts. As a result of these studies, US is increasingly being examined for its potential as a screening tool. The ongoing ACRIN 6666 study, funded by the Avon foundation and the National Cancer Institute, represents a definitive trial evaluating the potential of US as a screening tool.[7,8] However, its anticipated positive screening results could also highlight the difficulties of broad acceptance and replication of ultrasound screening exams, at the community level, due to the operator-dependent nature of conventional US. Furthermore, the ACRIN 6666 study does not specifically focus on improving the postscreening diagnostic accuracy of US.

Historically, efforts to improve the diagnostic accuracy of US have been carried out on two fronts. One approach is based on improving the current US devices and techniques which rely on reflection (or B-mode) imaging[9–11] while the second utilizes transmission imaging to characterize masses.

Stavros *et al.*[9] proposed that analysis of mass margins, shape and echo properties based on conventional US images could lead to highly accurate differentiation of benign masses from cancer (i.e., margin criteria). These observations also led to the development of the Breast Imaging Reporting and Data System (ACR-BIRADS) by the American College of Radiology, specifically for US. Early attempts to develop large aperture reflection tomography[12,13] (e.g., Norton and Linzer, 1979 and Carson *et al.*, 1981) did not have the benefit of Stavros' later results.

In 1976, Greenleaf *et al.*[14] made the seminal observation that acoustic measurements made with transmission US could be used to characterize breast tissue. On the basis of these studies they concluded that using the parameters of sound speed and attenuation (henceforth *transmission parameters*) could help differentiate benign masses from cancer. Using a number of *in vitro* samples of various types of breast tissue, they were able to quantify the sound speed (propagation velocity of an US pulse passing through the tissue) and attenuation (the reduction in pulse amplitude as it propagates through the tissue). They then demonstrated that, in a plot of sound-speed as a function of attenuation, the benign and malignant masses were well separated. As a direct result of this and other similar studies, a number of investigators developed transmission US scanners in an attempt to measure transmission parameters and to replicate their results *in vivo*. Examples include the work of Carson *et al.* (U. Michigan),[13] Andre *et al.* (UCSD),[15] Johnson *et al.*[16] (TechniScan Inc.), Marmarelis *et al.* (USC),[17] Liu and Waag (U. Rochester),[18] and Duric *et al.*[19–26] (Karmanos Cancer Institute).

The evidence cited above has led other investigators to appreciate the importance of multiple diagnostic criteria and high-quality imaging in increasing the diagnostic accuracy of US. The most recent findings in this area support and extend this concept by showing that computer aided detection can further increase the accuracy of the Stavros method by reducing (though not eliminating) operator dependence (e.g., Medipattern Inc.[27]). Furthermore, Technisan Inc. has shown that transmission parameters can be imaged effectively *in vivo*.[28] Our own studies have contributed to this contemporary body of knowledge by showing that a wide range of diagnostic criteria can be imaged with US tomography.[26]

Although the work cited above provides convincing evidence that US has great potential for improving the specificity over mammography, little progress has been made in demonstrating this advantage in the clinic. For example, the work of Andre *et al.*[17] clearly showed that operator-independent, *in vivo* transmission imaging of the breast was possible, demonstrating clear breast architecture. However, their work stopped short of imaging breast lesions. Techniscan, on the other hand, has demonstrated that operator-independent, *in vivo* imaging of breast lesions is possible.[29] They also demonstrated the ability to measure the Greenleaf parameters. However, they do not collect reflection data and therefore do not measure the margin criteria. Conversely, Stavros *et al.* have demonstrated *in vivo* differentiation of masses on the basis of reflection imaging but the results are operator dependent and they do not measure transmission parameters. Although the approaches differ, these groups have argued that further progress in this field will require fast clinical scanners, operator independence, and the ability to image multiple parameters. We are in complete agreement with these observations. Our own work with an early prototype[25] led us to the same conclusion. To address this gap in the knowledge base, our long term plan is to develop a scanner with the clinical goal of reducing the rate of biopsies for benign lesions. Our approach is based on the recognition that a device that is capable of *both* reflection and transmission imaging can measure both *margin criteria* and *transmission parameters* of attenuation and sound speed. Such a device has the potential to provide greater diagnostic accuracy than those utilizing either approach separately. As a first step in achieving our goal, we describe the development of an *in vivo* clinical scanner and the first clinical results showing simultaneous reflection and transmission *in vivo* imaging of the breast.

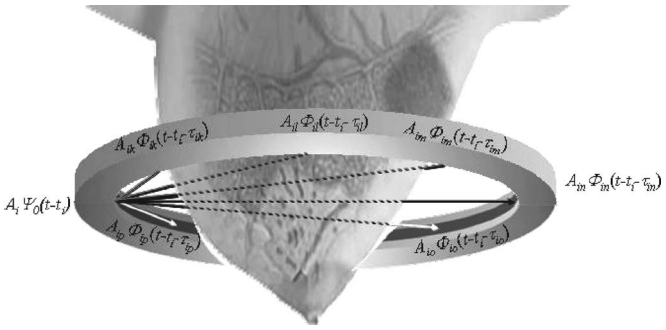

FIG. 1. A schematic representation of the CURE ring transducer. For a given transmitted pulse, a large number of received pulses are recorded. The ring insonofies a cross-sectional plane of the breast which leads to data that can be used to reconstruct images of acoustic properties.

II. GENERAL METHODS

In a previous paper, we described a laboratory prototype and presented results from phantom and *in vitro* studies.[25] Based on those results, we have designed and constructed a clinical prototype suitable for *in vivo* studies. We have developed the Computed Ultrasound Risk Evaluation System (CURE), based on the principles of US tomography.[19–26] This clinical prototype is a near real time device that has been integrated into the normal patient flow of the Walt Comprehensive Breast Center located at the Karmanos Cancer Institute, Wayne State University. A description of the CURE device is now presented.

A. Principles of operation

General principles

Consider the diagram in Fig. 1 in which a ring-shaped transducer surrounds the breast. The ring consists of 256 equally spaced elements each of which is capable of independently transmitting and receiving US signals. A signal generator is used to define a pulse shape, $\Psi_0(t)$. In the studies presented in this paper a one-cycle sinusoid was used.

The transmitting transducer elements are then sequentially driven with that pulse resulting in transmit pulses, $A_i\Psi_0(t-t_i)$ for $\{i=1,\ldots,256\}$, that are emitted in fan beams toward the opposite side of the ring. Interaction with tissue and water, as well as geometric dilution leads to a modification of the original signal by the time the receiving elements are reached. Thus for each transmit pulse there is a set of received pulses, characterized with different shapes, amplitudes, and arrival times and given by: $A_{ij}\Phi_{ij}(t-t_i-\tau_{ij})$ for $\{j=1,\ldots,256\}$, where $\Phi_{ij}(t)$ is defined to be a normalized, time varying waveform so that the amplitude A_{ij} is the received amplitude and τ_{ij} is the propagation time delay for each transmit-receive pair (i,j). Figure 1 shows schematically the relationship between the emitted and received pulses. The known quantities are the transmitted amplitudes A_i and transmit times t_i while the measured quantities are the matrices of received amplitudes A_{ij} and propagation time delays τ_{ij}. Comparison of the measured quantities with the known quantities and knowledge of the shape and size of the ring form the conceptual basis for interpreting the physical properties of the insonofied volume. Measurements of the amplitudes and time delays of the first signals to arrive at the receiving elements are used to construct images of attenuation and sound speed, respectively, while measurements of time delays of later arriving signals are used to construct reflection images, as described below. For N elements there are $N(N+1)/2$ independent transmit-receive pairs. Thus, for $N=256$ there are nearly 33 000 such pairs in our system. The volume is well insonofied thus enabling tomographic reconstructions of high-resolution reflection and transmission images, as described below. By translating the ring in the vertical direction it is possible to image the entire volume of the breast, ranging from near the chest wall through the nipple region.

Using the general approach described above and setting $i=t$ to represent positions of the transmitters in our ring array and setting $j=r$ to represent the receivers, we describe the methods used to construct reflection and transmission images.

Reflection imaging

A signal emitted by a transmitting element is scattered by a point reflector onto receiving elements distributed along the ring, as shown in Fig. 2. For a ring of diameter R, the travel time of the pulse of a constant velocity v from any transmitter to any receiver is given by

$$\tau_{\mathrm{tr}}=\frac{\ell_1+\ell_2}{v}=\frac{1}{v}\sqrt{R^2+x_p^2+y_p^2-2x_px_r-2y_py_r}+\sqrt{R^2+x_p^2+y_p^2-2x_px_t-2y_py_t},$$

$$\tau_{\mathrm{tr}}=\frac{\ell_1+\ell_2}{v}=\frac{1}{v}[\sqrt{(x_p-x_r)^2+(y_p-y_r)^2}+\sqrt{(x_t-x_r)^2+(y_t-y_r)^2}], \quad (1)$$

where the transmitter is located at (x_t,y_t), the reflector at (x_p,y_p), and the receiver at (x_r,y_r).

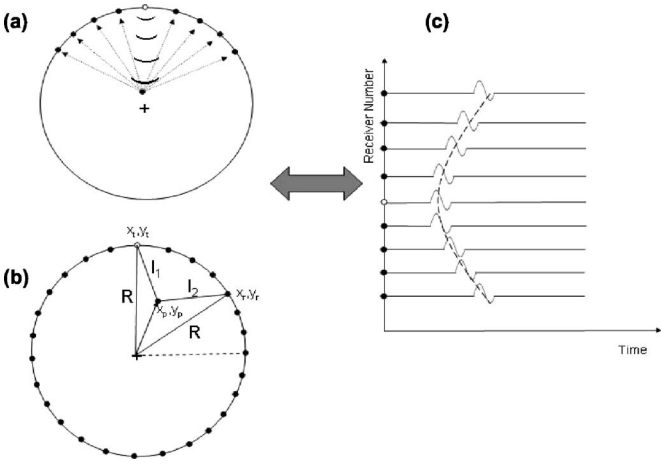

FIG. 2. Arrival times and the method of migration. (a) The relationship between transmitting elements (white circle), receivers (solid circles) and a scattering point, is shown. The center of the ring is marked with a "+" symbol. (b) The geometrical relationship between these quantities is shown. (c) A plot of receiver number as a function of time shows that the arrival times of an emitted pulse form a well-defined geometrical locus, as shown.

For a given (x_p,y_p) and (x_t,y_t) the arrival times are functions only of (x_r,y_r) and will form a locus such as the one shown in Fig. 2. Equation (1) predicts the pattern of signal arrival times, for each position within the insonofication plane. Kirchoff migration[29] is a method that can be used in conjunction with Eq. (1) to find all the reflecting surfaces in the insonofied plane. An image is constructed as follows.

(i) Create a grid consisting of $N\times M$ equally spaced pixels and a pixel size $\Delta x_p\times\Delta y_p$.
(ii) For each grid point, x_p, y_p, sum up all signal values that lie along the locus represented by Eq. (2). The resulting sum is a measure of the reflectivity of that point.
(iii) Repeat the process for all grid points and record their summed values.
(iv) Create image by assigning the summed values to each grid point.

The above method assumes that (i) reflecting surfaces are made up of point reflectors and (ii) that there are no multiple reflections. We have used this method to create two types of reflection images. To obtain the highest-resolution images we time the arrival of the time-domain signal. This approach yields high-resolution images that emphasize reflecting boundaries at the expense of echo texture. An example is shown in Fig. 3(a). In the second approach we fit envelopes to the time-domain signals and record the envelope arrival time [see Fig. 3(b)]. This approach creates a higher signal-to-noise reflection image that emphasizes echo texture at the expense of resolution.

Transmission imaging

In contrast to the reflection imaging it is possible to perform a computed tomography-(CT-) like reconstruction of sound speed and attenuation based on the signals that are

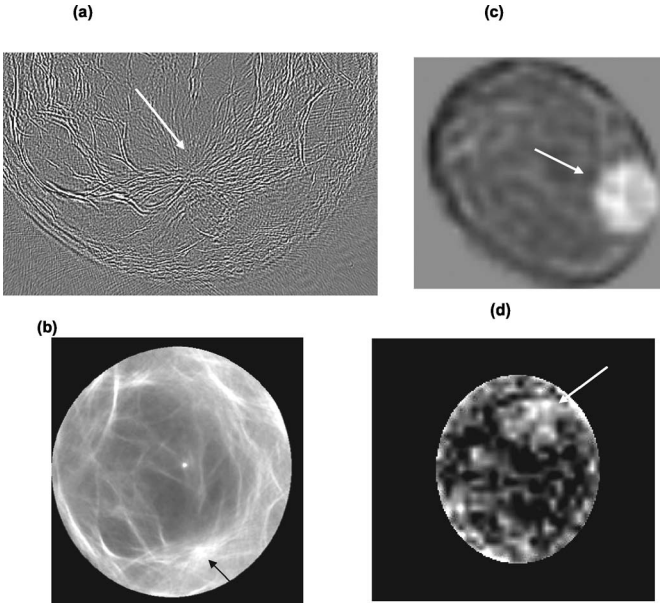

FIG. 3. Sample images illustrating different CURE imaging modalities. (a) High-resolution reflection image emphasizing detection of tissue margins. (b) Low-resolution reflection image emphasizing echo texture. (c) sound-speed image, and (d) attenuation image. Values increase from dark to white. The white arrows point to existing tumors.

transmitted through the breast tissue to the other side of the ring array. In a homogeneous medium the arrival times of a pulse emitted at a given transducer will arrive at the various receivers according to Eq. (2):

$$\tau_{\mathrm{tr}} = \frac{\sqrt{2}}{v}\sqrt{R^2 - 2x_t x_r - 2y_t y_r}, \tag{2}$$

where v is the propagation velocity of acoustic waves in that medium. In an inhomogeneous medium such as the breast, the arrival times will deviate from this expression because the acoustic velocity varies spatially within the medium [i.e., $v=v(x_p,y_p)$]. The deviations in arrival therefore can be inverted to obtain information about the sound speed changes in the insonofied plane. The inversion process can be described as follows.

The reconstruction is performed using a rectangular grid and within each of the grid cells we assume the sound speed/attenuation to be constant. Let the total number of cells be $N\times M$, corresponding to the number of pixels in the reconstructed image.

The sound travel time along a ray τ_{tr} can be represented as

$$\tau_{\mathrm{tr}} = \sum_{j=1}^{M}\sum_{k=1}^{N} l_{\mathrm{tr},j,k}\frac{1}{v_{j,k}},$$

where $l_{\mathrm{tr},j,k}$ is the length of this ray's path inside the cell j,k (if the ray does not cross this cell this value is zero) and $v_{j,k}$ the sound speed inside the cell. Let us assume that we have N_{tr} transmitter/receiver pairs (and correspondingly the same number of rays that cross the investigated medium). Up to 24 576 unique rays are possible with our system. Consequently, the distribution of sound speeds can be reconstructed by solving the system of N_{tr} equations

$$\left\{ \tau_{\mathrm{tr}} = \sum_{j=1}^{M}\sum_{k=1}^{N} l_{\mathrm{tr},j,k}\frac{1}{v_{j,k}} \right. .$$

In practice, it is difficult to measure the absolute arrival time precisely. Instead, we measure the arrival times relative to what would be expected in a homogeneous medium [as predicted by Eq. (2)]. Consider an initial homogeneous model such that

$$\left\{ \tau^0_{\mathrm{tr}} = \sum_{j=1}^{M}\sum_{k=1}^{N} l_{\mathrm{tr},j,k}\frac{1}{v^0_{j,k}} \right. .$$

Subtracting the model system from the above system of equations yields

$$\left\{ \tau_{\mathrm{tr}} - \tau^0_{\mathrm{tr}} = \sum_{j=1}^{M}\sum_{k=1}^{N} l_{\mathrm{tr},j,k}\left(\frac{1}{v_{j,k}} - \frac{1}{v^0_{j,k}}\right) \right. ,$$

which represents arrival time differences that we can measure. Letting $b_{j,k}=\frac{1}{v_{j,k}}$, the above can be re-expressed as

$$\left\{ \Delta\tau_{\mathrm{tr}} = \sum_{j=1}^{M}\sum_{k=1}^{N} l_{\mathrm{tr},j,k}\Delta b_{j,k} \right. .$$

Typically, the number of equations in this system exceeds the number of unknowns. We therefore utilize a minimization approach to find a stable solution which yields an image of the sound speed distribution. The same principle can be applied to determine amplitude changes $(A_{\mathrm{tr}}/A^0_{\mathrm{tr}})$ yielding images of attenuation. Figures 3(c) and 3(d) show examples of sound speed and attenuation images.

Physical interpretation of the reconstructed images

In order for the reconstructed images to have clinical value, it is necessary to relate the image reconstructions, defined above, to physical quantities associated with the insonofied medium. From a mathematical point of view the above discussion represents relatively simple methods of solving an inverse problem. In this case we have solved for the physical parameters of reflection, sound speed, and attenuation of the insonofied volume from measurements made on a cylindrical surface, swept out by the moving ring. The accuracy of the derived parameters depends on the assumptions used to make the solution of the inverse problem tractable. The results presented in this paper are based on a relatively simple model of scattering physics that assumes straight ray propagation and single scattering events. Our use of very low ultrasound frequencies, centered on 1.5 MHz, is aimed at minimizing the complications associated with

strong scattering and thereby justify the simplifying assumptions made in the above discussions. Nevertheless, these assumptions limit the interpretation of the physical quantities derived by these methods. Thus, the physical interpretation of the reflection images is that they map out the reflecting surfaces that mark the boundaries of various tissue types. They do not represent directly the reflectivity of these tissues. Similarly, sound speed images are determined on the assumption of straight ray propagation. Consequently, the reconstructed images represent a smoothed-out version of the true sound-speed distribution, limiting the spatial resolution to the values quoted in this paper. Similar consideration applies to the attenuation images which do not take into account out-of-plane scattering. The resulting images map out relative attenuation only. We believe that this level of interpretation is a good starting point for the proof-of-concept study presented here. Results from more sophisticated solutions of this inverse problem will be presented in future papers. Readers requiring further mathematical details of this inverse problem are referred to a number of excellent reviews that can be found in the literature.[30,31]

Clinical value

An advantage of the ring design is that it allows the capture of most of the planar scattered field which allows the construction of multiple diagnostic images, as described above. A multiplicity of contiguous coronal images, each one containing independent clinical information, is necessary to maximize the clinical value of the data collected by CURE as described below.

Echo-texture reflection imaging. Reflection imaging, performed by migrating the envelopes of the propagating signals, as described above, yields echo-textured reflection images. A set of such images provides echo-texture data for the entire breast, ranging from the chest wall to the nipple region. The clinical value of mapping tissue changes in echogenicity lies in the discrimination of the *relative* internal characteristics of a mass from the normal background tissue echogenicity. For example, a low echogenicity mass (i.e., hypoechoic) can be detected against a background of higher echogenicity (i.e., hyperechoic) parenchyma, or fat. Therefore, such mass detection can occur even if the imaging resolution is not sufficient to further characterize the mass using margin criteria. In fact, most cancers do not have any specular reflectors at the interface with adjacent tissue. Therefore current margin criteria are only effective due to the resolution of high-frequency (e.g., 10–14 MHz), linear array transducers favored by breast imagers. While echo-textured reflection images of CURE support the future use of margin criteria as resolution improves, their main role for the current prototype is to document the relative echogenicity over normal background tissue.

Edge detection reflection imaging. Migrating the time-dependent signals directly, yields high-resolution images of reflecting tissue boundaries. This imaging modality trades off echo texture for resolution. It is designed to accurately map dominant specular reflectors in tissues, such as Cooper's ligaments and fibrous bands within normal breast tissue. This may also include mass margins if a smooth specular reflector is involved, such as a cyst wall or the capsule of a benign mass (e.g., fibroadenoma). Perhaps more importantly, it provides an opportunity to visualize the reaction of adjacent tissue with masses, in the form of spiculation and architectural distortion for example. While cancers do not have specular reflectors on their margins, their three-dimensional (3-D) effect upon surrounding tissue provides important additional characteristics that also make up BIRADS margin criteria.[9]

Sound speed imaging. The arrival times of acoustic signals can be used to construct maps of the sound-speed distribution. A stack of such coronal images provides data for the entire breast. *In vitro* studies, described in existing literature (e.g., Greenleaf[14]), have shown that cancerous tumors have enhanced sound speeds relative to normal breast tissue. These appear related to underlying tissue densities and surrounding tissue "stiffness." The sound-speed difference of tumors over fat is even greater, leading to potential characterization of masses in even heterogeneously dense breasts, assuming sufficient accuracy.

Attenuation imaging. Even in current reflection imaging, attenuation characteristics of a mass, such as shadowing and "through transmission," help in differentiating cancer from benign tumors. Similar to sound speed, higher attenuation in cancer also relates in part to tissue density and relative interaction with adjacent tissue, causing either greater absorption or scatter of the US wave. Tomographic reconstructions based on amplitude changes of the signals result in attenuation images. A set of such images provides attenuation data for the entire breast.

Image fusion. CURE reflection and transmission images are inherently coregistered since they are constructed from the same data, resulting in straightforward fusion images without geometric discrepancies. These superimposed imaging sequences can be evaluated for either improved visualization (e.g., a high-sound-speed focus may better detect a lesion from the background) and/or characterization (e.g., reflection may then show mass boundaries better). Just as PET/CT scanning offers a composite of functional imaging superimposed upon the anatomic background, the current CURE fusion process similarly displays a superposition of different tissue information for the same region.

The above imaging modalities define the diagnostic capabilities of CURE. Other factors can also enhance the clinical utility of CURE and these are summarized as follows.

Whole-breast analysis. Since CURE images the whole breast it is possible to extract diagnostic information from the entire volume of the breast. This is possible, even with a ring array because the imaging bed is highly flexible and allows the breast, some of the axilla, and underlying chest wall to sufficiently protrude through the ring in a dependent position.

Nonionizing imaging. X-ray imaging is considered to pose a radiation risk, even with the low levels associated

with mammography.[3] US eliminates that risk and allows essentially unlimited repeats of exams, thereby making it possible to easily monitor changes in the breast.

Noninvasive Imaging. Unlike some modalities like CT and MRI, CURE is not dependent upon the use of contrast agents for tissue differentiation and is therefore completely noninvasive.

Reduced operator dependence. With tomographic imaging, CURE minimizes operator dependence by suspending the breast in a water bath and imaging the breast in virtually the same coronal plane for each study. No direct transducer contact with the skin is required in the current prototype. Reproducible images from multiple exams can thus be more easily compared in order to search for any volumetric changes.

B. Basic system architecture

Ring transducer system

All of the above clinical advantages would be compromised if there is patient movement during a scan. The essential requirement for minimizing motion artifacts is to design a transducer and data acquisition system that performs a whole breast scan in one breath hold and a single slice scan faster than a cardiac cycle. A target goal of less than 1 minute for the former and 0.1 s for the latter was established. To achieve these goals we chose to make a solid-state ring transducer obviating the need for rotational motion. As a result, the only limiting factor in the sequences of transmits and receives is acoustic travel time across the ring and back. For a 20 cm ring, immersed in water and operating at 1.5 MHz the required "wait" time between firings was approximately 300 microseconds. In order to achieve this design goal it was necessary to utilize a solid-state ring in conjunction with massively parallel data acquisition. We chose to implement a data acquisition system in which one channel was dedicated for each transducer element. In our case, 256 elements and 256 associated data acquisition channels were used. The ring transducer was placed on a gantry that allowed for translational motion in order to scan the whole breast. The drive mechanism was designed to push the transducer at a rate of ~10 mm/s. For a breast 20 cm in length, the mechanical scan can be carried out in about 20 s. The electromechanical properties of the ring transducer are summarized in Table II.

The patient bed

The patient table contains the water tanks, the circular transducer and transducer drive system, the data acquisition system, and all necessary accessories and controls. Panels are removable in order to access and service the internal components. A picture of the prototype is shown in Fig. 4. An open tubular frame with a tensioned sailcloth patient suspension surface is used in order to provide maximum access to the patient's breast and chest wall. This approach offers more flexibility than a traditional hard table. Patient comfort is maximized given that the duration of the procedure is less than 1 minute. The patient is required to climb two or three steps to get onto the patient suspension surface.

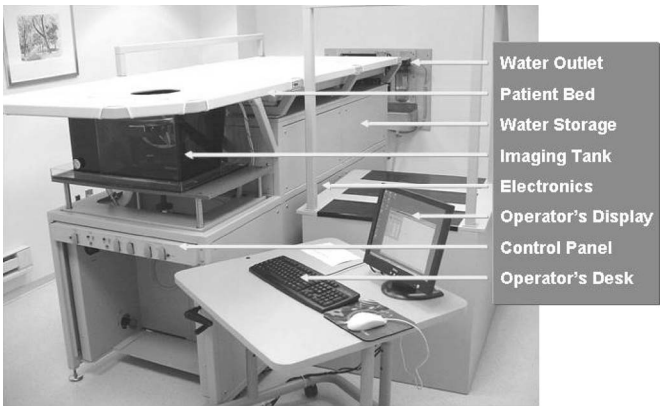

FIG. 4. System workstation and prototype patient bed. The workstation is used to set the scanning parameters. The patient lies on the bed, in the prone position, with the breast suspended through a hole in the table, in the water tank just below the table surface. The various components of the system are labeled.

The imaging tank

The water tank under the bed contains the ring transducer assembly and the associated mechanical subsystem for positioning the transducer. A single hole in the middle of the bed allows the patient's breast to be suspended in the water bath. The table height is sufficiently high (approximately 48 in.) to allow the system operator to be seated while visually positioning the transducer along the patient's breast. The water tank is clear so as to allow visual position feedback. The ring transducer support has only vertical motion capability. Since the CURE device does not require compression, horizontal centering is accomplished by minor movement of the patient. The water tank system is illustrated in Fig. 5.

The water tank system includes provisions for a number of items necessary for water and health management, similar

FIG. 5. (a) Imaging tank. The water tank that contains the ring transducer is referred to as the imaging tank. Its temperature is controlled with a heater and is usually set to body temperature. (b) The ring transducer is immersed in water during the scan. It is connected to the electronics under the table via two cables, as shown.

to a pool or spa. The imaging tank consists of a full inner tank and a slightly bigger outer tank to collect water overflow. A rectangular construction was chosen over a circular geometry in order to minimize focused reflections. Water recycling, fill, drainage, and cleaning, with associated pump and flow control systems, are part of the water management system. Water temperature control is achieved by an electrical heater, both for patient comfort and experimental consistency. The height of the water tank is manually adjustable and the interface between it and the table uses watertight bellows and gaskets. This allows for the varying curvature of chests and the size and weight differences among patients. Water is pumped into and out of the primary exam water tank from a storage tank within the table. Water temperature is automatically controlled to approximately equal body temperature. There is sufficient thermal mass in the water to maintain essentially a constant temperature for the duration of the scan. By design, the water temperature does not vary by more than 0.2 °C during the data acquisition of any slice within the breast scan. The water temperature is monitored and is provided with the scan data to the image reconstruction algorithms.

System back end

The back end of the prototype system consists of a "standard" Intel-based computer board in compact PCI form factor. These computer board configurations support standard, commercial network and computer systems and software to allow networking with the reconstruction/display workstation. The onboard computer provides key control functions for setting up the CURE exams, such as the scan time and the spatial and time interval between scans. It also controls the flow of data from the CURE device to the image reconstruction computers, as described below.

Data processing

Since the CURE imaging methodology is closer to that of CT and MRI, the data acquisition and image reconstruction are quite different from that used in conventional US. In contrast to conventional US, CURE records include a large fraction of the scattered field. As Fig. 3 shows, a CURE exam yields four tomographic images per volume slice, leading to four different types of image stacks, representing the entire volume of the breast whereas conventional US provides detailed, real time views of smaller targeted volumes in only one reflection modality.

The raw data are obtained by sampling the received signals at a rate of 6.25 MHz. The sampled signals are recorded and stored in time series records in a large 11 GByte memory cache. The memory is read out after the completion of the CURE exam and the resulting records are transferred to the image reconstruction computers over a 1 GBPS fiber optic link and stored on local hard drives. The reconstruction software reads and analyzes the stored records and outputs the four types of images previously described.

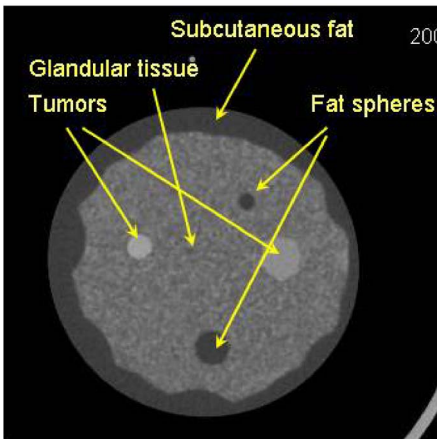

FIG. 6. The breast phantom. A CT cross-sectional image of the breast phantom shows two fatty inclusions (dark), two "tumors" (white), imbedded in glandular tissue (gray). A layer of subcutaneous fat lies just below the skin of the phantom (dark).

III. RESULTS

The prototype system was installed in August, 2005 at KCI's Alexander J. Walt Breast Center. CURE was integrated into the patient flow of the center, in order to facilitate clinical studies. We now describe the phantom and *in vivo* studies carried out with CURE.

A. Phantom study

CURE was first evaluated with phantoms in order to characterize its performance. The breast phantom was built by Dr. Ernest Madsen of the University of Wisconsin and provides tissue-equivalent scanning characteristics of highly scattering, predominantly parenchymal breast tissue. A representative x-ray CT scan of the phantom is shown in Fig. 6. The phantom mimics the presence of benign and cancerous masses embedded in glandular tissue, including a subcutaneous fat layer. The phantom contains eight masses ranging in size from 6 to 15 mm. The phantom was scanned with CURE and representative images are shown in Fig. 7.

In order for CURE to have clinical relevance and given our specific goals, the device should be able to detect all masses that can be biopsied under US guidance. In practice

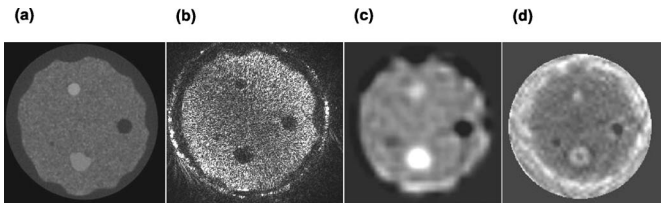

FIG. 7. CURE imaging of the breast phantom. From left to right: (a) an x-ray CT slice containing two fat spheres and two "cancerous tumors." The corresponding CURE images show (b) reflection, (c) sound speed, and (d) attenuation. All four masses are detected in the three CURE images. Note the significantly different sound speed and attenuation of the benign and cancerous masses (c and d). The masses range in size from 6 mm to 15 mm. The qualitative intensity scale ranges from dark (low values) to white (high values).

TABLE I. Sound-speed performance of CURE.

Material	Known sound speed (m/s)	Measured sound speed (m/s+/−SD)	Difference sound speed (m/s+/−SD)
Subcutaneous fat	1470	1470+/−10	0+/−10
Fat spheres	1470	1465+/−5	5+/−5
High attenuation tumor	1549	1555+/−5	6+/−5
Irregular tumor	1559	1565+/−15	6+/−15
Glandular	1515	1513+/−3	2+/−3

this means being able to detect and characterize masses 5 mm in size or larger. The phantom study has demonstrated the ability to detect all masses including those as small as 6 mm in size. Furthermore, the masses were detected in all four imaging modalities, demonstrating the ability to characterize as well as detect masses in the clinically relevant mass range.

The reconstructed images of the phantom were analyzed in order to quantify the system performance. The phantom mass assessment showed a resolution of 0.5 mm in reflection and 4 mm for sound speed and attenuation. The detection contrast was >3 (SNR) for all masses in all modalities and the tumor location accuracy was ±3 mm. The sound speed characterization of the various phantom components indicated an accuracy of 5 m/s per pixel (Table I). The absence of *a priori* knowledge of the phantom attenuation, at our frequency, prevented calibration of the attenuation accuracy and we leave the reporting of that to a future paper. The overall technical performance of CURE is summarized in Tables I and II.

The system performance was largely as expected. The in-plane spatial resolution, limited mainly by the central operational frequency, reached the expected $\lambda/2$ value of 0.5 mm when migrating the RF signals. The in-plane resolution for sound speed and attenuation imaging, on the other hand, is defined by the density of rays (a ray is defined as a line connecting each transmit-receive pair). The latter is defined by the spacing of the 256 elements along the 20 cm ring. The resulting ray density is insufficient to fill cells smaller than about 2 mm hence limiting the pixel size of the reconstructions to about 2 mm. Consequently, the resolution for transmission imaging was limited to ~4 mm. The out-of-plane resolution is defined by the 12 mm elevation beamwidth of the transducer elements. Consequently, masses smaller than ~12 mm present reduced per-pixel, in-plane contrast relative to larger masses (Fig. 8). Nevertheless, the phantom studies indicated that masses down to 6 mm in size could be detected. Overall, CURE performance in the phantom study justified proceeding with *in vivo* testing, described in the next section.

TABLE II. Summary of CURE performance characteristics.

Item	Performance
Operating center frequency	1.5 MHz
Number of transducer elements	256
Number of data acquisition channels	256
Data acquisition time (one slice)	100 ms
Data acquisition time for entire slice set (45 slices)	45 s
Spatial resolution (reflection, in plane)	0.5 mm
Spatial resolution: sound speed and attenuation	4 mm
Out-of-plane resolution	12 mm
Minimal detectable sound speed variations	5 m/s

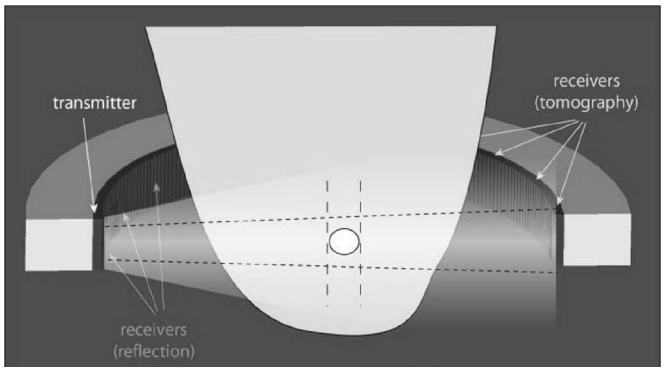

FIG. 8. A 5 mm mass in a 10 mm beam. The ring transducer is characterized by a finite beam thickness as measured in the vertical direction (normal to the ring plane). The smaller the object relative to the beam width, the more difficult it becomes to detect because its signal is being averaged out by competing signals from above and below the object.

B. *In vivo* study

The objective of this portion of the study was to assess the performance of CURE under *in vivo* conditions. The performance assessment goals were to demonstrate (i) *in vivo* imaging of breast architecture and (ii) detection of breast masses larger than 1 cm in size. The restriction of mass sizes to 1 cm and larger was based on the ~1 cm elevation beamwidth of the ring transducer as described in Sec. IV (see also Fig. 8). The results of the performance assessment are described in this section. All imaging procedures were performed under an Institutional Review Board (IRB) approved protocol and in compliance with the Health Insurance Portability and Accountability Act (HIPAA).

Methodology

The results for the initial clinical group of patients are presented here. Clinical details of this study will be provided in a separate paper. An outline of the imaging procedure is as follows. The patient is positioned on the bed with the pendant breast suspended in the water bath. The ring transducer, which encircles the breast, is raised against the chest wall under operator control. The operator then sets up the scan parameters using the keyboard/monitor at the patient table. Once the operation mode has been set, data acquisition is initiated by the operator. The system automatically acquires each image slice of the breast and automatically translates the ring probe for acquisition of the next programmed slice. The entire acquisition process for a breast takes less than one minute. After acquiring the complete data set for a patient,

the data are transferred to the PC workstation for reconstruction and viewing. Although the system was designed to acquire the necessary data in one breath hold, breath holding was not implemented because the effects of breathing were negligible in any given slice. Future studies that focus more on volumetric reconstructions may require patients to hold their breaths.

Data for 65 patients were acquired in this way. Technical malfunctions related to memory buffer corruption and hard drive failures led to the loss of 14 data sets. Consequently, 51 data sets were available for study at the conclusion of the accrual process. Furthermore, an additional 7 patients were found to have no mass so that the number of data sets available for imaging masses was 44. Typically 45 tomographic data slices were collected per patient. Each data slice was reconstructed to produce images of reflectivity, sound speed, and attenuation. Qualitative results from the images are described below for brevity.

CURE imaging of breast architecture

The phantom results provided a calibration for CURE'S intrinsic imaging capabilities. To validate this imaging capability *in vivo* where confounding biological factors, such as heterogeneity of tissue and greater "structure" noise may play a role, we analyzed our images for the presence of breast architecture such as fibrous stroma, glandular tissue, fatty tissue, and masses.

Fibrous stroma. The phantom results provided confidence that the CURE system provides realistic rendering of simulated masses without introducing major artifacts. However, the breast phantom that was used in our study does not contain analogues to breast fine structure, such as fibrous stroma, Cooper's ligaments, and ducts, features which are apparent in mammograms. We therefore analyzed our CURE images to ascertain the presence of such structures.

Figure 9 presents a CURE reflection reconstruction. A total of 15 CURE tomograms were stacked using a maximum intensity projection, in *ImageJ*, in order to create a "CURE mammogram." The stack represents a layer of the pendant breast that is about 4 cm thick. The fibrous, wispy structure evident in conventional mammograms is also present in the CURE images. The central white dot is a reconstruction artifact which we are planning to eliminate in the next stage of our algorithm development. On the basis of such images, we have concluded that CURE reflection imaging is sensitive to similar structures seen in mammograms. The spatial resolution in the CURE reflection images ranges from 0.5 mm to ~1 mm. The intensity scale on these images is indirectly related to reflectivity because it describes the relative strengths of reflection echoes. However, the 2-D approximation that is used for image reconstructions does not allow a proper calibration of the absolute reflectivity. Nevertheless, these images reveal the distribution of reflecting surfaces in the breast.

Fibrous stroma owes its conspicuity to its highly reflective nature which can be explained by theory. Consider a US pulse impinging on a breast fiber. In the case of normal incidence, the reflected energy is related to the change in acoustic impedance, as follows:

$$R = \left[\frac{Z_2 - Z_1}{Z_2 + Z_1}\right]^2,$$

where Z_1 is the acoustic impedance of the fibers relative to the background tissue Z_2. Since $Z_1 \gg Z_2$, $R \rightarrow 1$ and the fibers reflect much of the US energy incident on them. Thus, they are prominent in our reflection images because of the sudden changes in acoustic impedance that they represent.

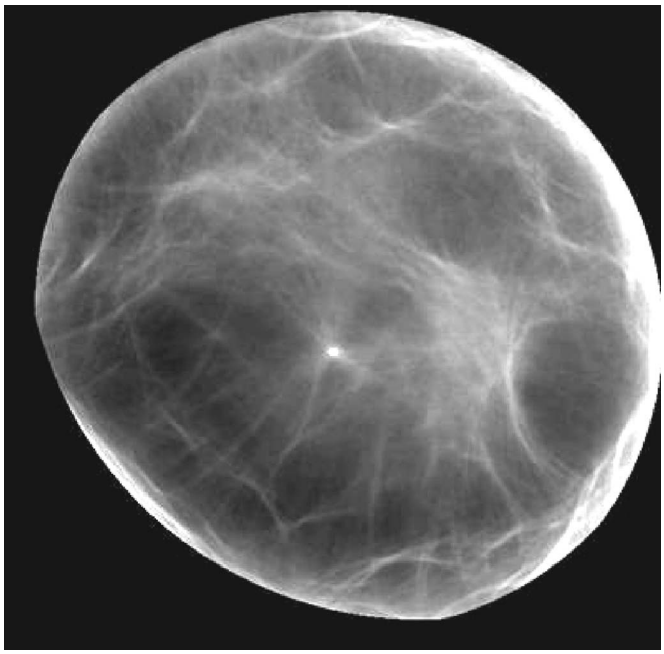

FIG. 9. Sample reflection image showing detailed breast architecture. Although the CURE view is cross sectional and therefore represents a different perspective compared to mammography, it is evident that fibrous stroma are visible in the CURE image.

Glandular and fatty tissue. In order to maximize the diagnostic potential of CURE, it must be capable of imaging a variety of tissue properties. Figure 10 shows sample images of reflection, sound speed, and attenuation. The sound-speed images are calibrated on an absolute scale. The units are meters/second, as shown on the images. An absolute calibration is possible in this case because the arrival times are compared to those in water, whose sound speed is known at the time of the scan. In the case of attenuation images, only a relative calibration is possible because amplitude changes result from 3-D scattering whereas our codes are limited by the assumption of a 2-D geometry. As noted earlier, the spatial resolution of our sound speed and attenuation images is about 4 mm. At this resolution we do not expect the system to be sensitive to the fibrous structure of the breast. However, as the images indicate, fatty and glandular tissues can be characterized. This patient also has a 3 cm invasive ductal carcinoma (IDC), which is evident in all CURE modalities.

In our sample of patients we have imaged a wide variety of breast types, ranging from fatty to dense on the BIRADS

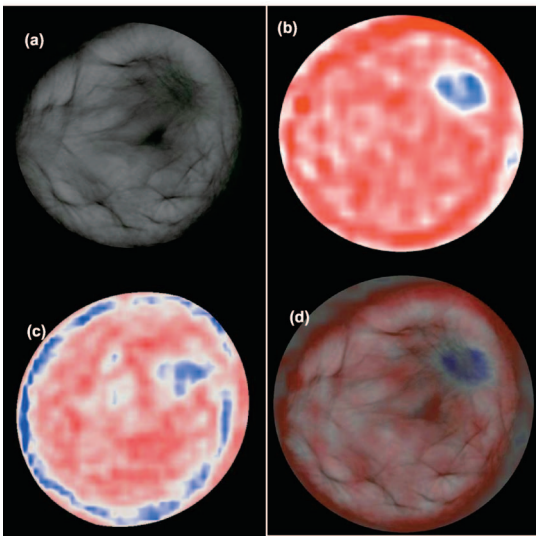

FIG. 10. Multimodality CURE imaging. (a) CURE reflection image showing a tumor and associated architectural distortion. (b) Sound-speed image showing the tumor as a high-sound-speed mass. (c) Attenuation image showing the tumor as a highly attenuating mass. (d) A superposition of a reflection image on a sound-speed image. The latter illustrates the interaction of fibrous stroma with the tumor. The gray scale represents values increasing from white to dark. The color scale has values increasing from red to blue.

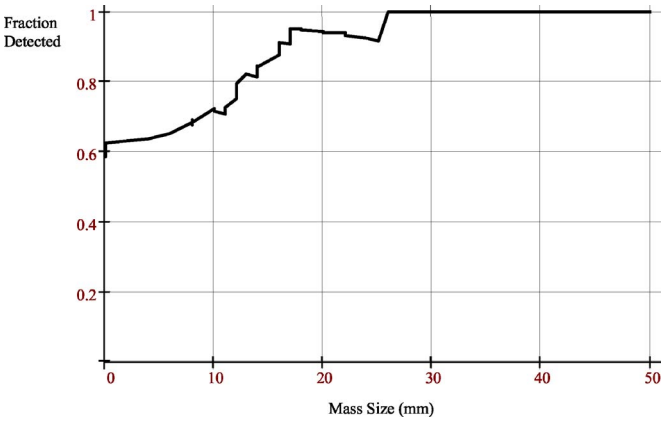

FIG. 11. The mass detection rate. The cumulative fraction of masses detected is plotted as a function of mass size. The graph shows that ~90% of masses >15 mm in size are detected in our sample of patients.

classification scheme. By taking whole breast averages for the fatty and dense samples, we have been able to estimate the average acoustic properties of fatty and glandular tissues separately. As an example, we have found that the sound speeds of fatty and glandular tissue are 1408±17 and 1472±37 m/s, respectively. The sound-speed values were calibrated by comparing the measured arrival times with those in a water tank containing only water of known sound speed. Despite a large variation of sound speeds within each group, the two tissue types are separable by sound speed, indicating that acoustic characterization of breast tissue is feasible.

Sound-speed differences arise because of differences in tissue density and tissue compressibility. The relationship between these properties is given by

$$V = \sqrt{\frac{c}{\rho}}$$

where V is the sound speed of the tissue, c is the bulk modulus, and ρ is the density. Glandular and fatty tissue are separable in CURE sound-speed images because they have intrinsically different amounts of compressibility relative to their density.

At our frequency of 1.5 MHz, attenuation is caused mainly by scattering resulting from an inhomogeneous distribution of acoustic impedance. Generally, glandular tissue has greater attenuation compared to fatty tissue.

Breast masses. Since the long-term clinical goal of CURE is to identify and differentiate masses we must first demonstrate the ability to image and localize a wide variety of masses. Using the multimodality aspect of CURE, we have searched for breast masses based on locations inferred from mammography and US exams. The masses were then identified in the CURE images if their locations corresponded to the radial and clock positions estimated by standard imaging. Further clinical analysis is beyond the scope of this paper and will be reported in more detail in a future paper.

As noted in the previous section, we have demonstrated the ability to image breast architecture. In the case of breast masses, we have found that a wide variety of masses can be imaged with CURE and that most masses larger than 1 cm in size can be detected in one or more of CURE's imaging modalities. As anticipated, detection is limited by the size of the mass. Figure 11 shows a plot of masses detected as a function of mass size. As expected, CURE performance declines as the mass size drops to 1 cm and below. These observations confirm our prediction that limited out-of-plane resolution leads to limited in-plane contrast. Consider Fig. 8. A mass smaller than the width of the elevation beam suffers from signal dilution because signals associated with the mass are now being measured in the presence of structure noise (i.e., unwanted signals from surrounding structure). This beam dilution leads to a loss of contrast which progressively worsens as the mass size shrinks relative to the elevation beam width. In Fig. 11 it can be clearly seen that as the mass size approaches the elevation beamwidth (~1 cm) the detection rate drops dramatically such that only 70% of the masses larger or equal to 1 cm in size are detected. Documentation of this effect has allowed us to redesign the transducer with the goal of improving the elevation resolution and increasing the mass detection rate.

IV. DISCUSSION

A. CURE performance

As summarized in Table II, the acquisition time per slice is about 0.1 s. Consequently both cardiac and breathing movements are effectively frozen in any given slice. The corresponding images show no trace of motion artifacts. The total data acquisition time (the time required to acquire all

TABLE III. CURE *in vivo* imaging performance.

Item	Performance
Spatial resolution (reflection, in plane)	0.5 mm
Out-of-plane resolution	12 mm
Minimal detectable sound-speed variations	5 m/s
Minimal detectable variations in attenuation	10%
Total patient exam time	5 min
Data throughput time	90 min

slices that correspond to the breast exam) was typically 45 s. Although this is well below the capability of CURE, we took a conservative approach by waiting one second between slices in order to minimize effects of reverberations and mechanical vibrations. However, even with a 45 s data acquisition time there is no apparent blurring due to motion. Occasionally, we see evidence of breathing by detecting movement during a series of slices but we can assume that the breathing is frozen in any individual slice. Hence motion artifact would be an issue only in stacking images, which in turn can be obviated through conformal stacking techniques.

From the patient's perspective the CURE exam time is very short. The actual scan time is 45 s with less than 5 minutes required to set the patient bed and initial transducer position. Consequently, the patient is in and out of the exam room in about 5 minutes. However, the current data throughput time are significantly longer. The acquired data are stored in a large memory buffer. Transferring the data from the memory buffer to the image reconstruction computers takes about 90 minutes. This is the current bottleneck in the system, limiting the patient throughput to about 5 patients/day.

Summary of technical performance

We have assessed CURE's *in vivo* performance, by analyzing the reconstructed images and by tracking the data flow through the CURE system. The system performance is summarized in Table III.

B. Ability to measure cancer characteristics

The results described in Sec. III demonstrate that our technical goal of imaging masses >1 cm in size was largely achieved. The corresponding diagnostic goal is to image clinically relevant mass characteristics in support of the longer-term goal of differentiating benign masses from cancer using a combination of margin and transmission parameters. A first step in that direction is to demonstrate that masses can be imaged in both reflection and transmission CURE imaging. By definition, if a mass is detected in our reflection, sound-speed and attenuation images, we can measure both its margin and transmission parameters. As noted in the previous section, 75% of the masses >1 cm in size were detected by CURE in a combination of reflection and transmission imaging. In a future paper we will describe the development of a predictive model for differentiating cancer from benign masses, based on these parameters.

C. Comparison with standard modalities

From a technical perspective, mammography yields 2-D whole breast projection images. The images are not tomographic, but rather simple projections, hence the need to significantly compress the breast to minimize the superposition of tissues and thereby reduce structural noise. Heterogeneous parenchyma (i.e., structural noise) can prevent screening detection of cancer by mammography, particularly for women with dense breasts. Although standard US is well suited for follow-up imaging of lesions it requires advance knowledge of the lesion location. Furthermore, it is ill-suited for rapid, reproducible, whole breast imaging and, as a consequence of natural movement and the variation in sizes and textures of breasts, the operator's accuracy becomes a variable of the images, making it difficult to register images taken at different times.

The above limitations of mammography and US can be mitigated through the use of tomographic techniques; hence the recent research efforts in x-ray tomosynthesis and US tomography. Currently, the most frequently used tomographic technique for breast imaging is MRI. MRI, in combination with contrast agents, has been shown to be effective in detecting masses. Enhanced regions can show architectural distortion eminating from a well-defined focus that identifies the location of the mass. However, limited access prohibits its widespread use. Specificity of MRI (between 60% and 80%) appears better than mammography, but the long exam time (up to 1 hour) and high cost (typically $1,000 per exam) limits its routine use in screening and routine diagnostic follow-up.

CURE has the potential to provide the benefits of tomography at low cost, with no ionizing radiation, no contrast agents and with minimal impact on the clinical workflow. Furthermore, the speed of the scan minimizes motion artifacts, it requires no shielding (thereby reducing construction costs) and it is not dependent on the use of contrast agents. Currently, CURE's limited detection and image processing times stand in the way of fully realizing these advantages in the clinic. These limitations and proposed solutions are described below.

(1) *Limited detection*. CURE performs best for masses >1 cm in size. As noted above, this performance limitation is the result of limited out-of-plane resolution. Our current research is focused on improving the out-of-plane resolution from 12 mm to 5 mm, thereby improving the overall detection rate for masses <1 cm in size and allowing reliable and consistent detection and characterization of all masses.
(2) *Limited throughput*. Although the patient scan takes less than 1 minute, the data transfer and image reconstruction times limit the patient throughput to 5 patients per day. Our goal is to improve the throughput to 25 patients per day. The improvement in throughput will be achieved by reprogramming the routines for reading out the on-board memory, reducing the data acquisition volume by eliminating unnecessary acquisitions, and increasing the speed of the reconstruction algorithms.

Despite these limitations, CURE has met its initial goals of (i) reliable imaging of breast architecture and (ii) multimodality (reflection + transmission) imaging of breast masses. In a future paper we will describe the use of mass characteristics in differentiating cancer from benign masses.

V. CONCLUSIONS

Although mammography is the gold standard for breast imaging, it does lead to a high rate of biopsies of benign lesions and a significant false negative rate for women with dense breasts. In response to this imaging performance gap we have developed a clinical breast imaging device based on the principles of US tomography. The Computed Ultrasound Risk Evaluation (CURE) system has been designed with the clinical goal of whole breast, operator-independent imaging and differentiation of breast masses. In an initial assessment of its *in vivo* performance, we found the following.

(i) Tomographic imaging of breast architecture is feasible.
(ii) Short patient exam times (45 s).
(iii) Spatial resolution of 0.5 mm in reflection and 4 mm in transmission was achieved.
(iv) Masses >15 mm in size were routinely detected.
(v) Reflection, sound-speed, and attenuation imaging of breast masses was demonstrated.

These initial results indicate that whole-breast imaging and the detection of breast masses is feasible. Future studies will focus on improved detection and differentiation of masses in support of our long-term goal to improve the specificity of breast exams—the subject of a future paper.

ACKNOWLEDGMENTS

This study was made possible, in part, by grants from the National Institutes of Health (R43 CA108072-01 and R43 CA107910-1). The authors thank Linda Darga for her assistance with patient recruitment. Furthermore, the authors wish to thank the staff of the Alexander J. Walt Comprehensive Breast Cancer Center at the Karmanos Cancer Institute for their support during and after the construction of the CURE exam room and for their generous assistance with patient management.

[a]Author to whom correspondence should be addressed. Electronic mail: duric@karmanos.org

[1]D. A. Berry *et al.*, "Effect of screening and adjuvant therapy on mortality from breast cancer," N. Engl. J. Med. **353**(17), 1784–1792 (2005).
[2]P. C. Gotzsche and O. Olsen, "Is screening for breast cancer with mammography justifiable?," Lancet **355**, 129–134 (2000).
[3]G. F. Schwartz and S. A. Feig, "Nonpalpable breast lesions: biopsy methods and patient management," Obstet. Gynecol. Clin. North Am. **29**(1), 137–57 (2002).
[4]P. J. Littrup, A. Goodman, C. Mettlin, and Investigators of the ACS-NPCDP, "The benefit and cost of prostate cancer early detection," Ca-Cancer J. Clin. **43**, 134–149 (1993).
[5]P. J. Littrup *et al.*, "Cost-effective prostate cancer detection: Reduction of low-yield biopsies," Cancer **74**, 3146–58 (1994).
[6]T. M. Kolb, J. Lichy, and J. H. Newhouse, "Comparison of the performance of screening mammography, physical examination, and breast US and evaluation of factors that influence them: An analysis of 27,825 patient evaluation," Radiology **225**, 165–175 (2002).
[7]L. Lucas-Fehm, "Sonographic mammographic correlation," Appl. Radiology, **2**, 20–25 (2005).
[8]ACRIN website: www.acrin.org.
[9]A. T. Stavros, D. Thickman, C. L. Rapp, M. A. Dennis, S. H. Parker, and G. A. Sisney, "Solid breast nodules: use of sonography to distinguish between benign and malignant lesions," Radiology **196**, 123–34 (1995).
[10]R. R. Entrekin, B. A. Porter, H. H. Sillesen, A. D. Wong, P. L. Cooperberg, and C. H. Fix, "Real-time spatial compound imaging application to breast, vascular, and musculoskeletal ultrasound," Semin Ultrasound CT MR **22**(1), 50–64 (2001).
[11]R. S. Shapiro, W. L. Simpson, D. L. Rausch, and H. C. Yeh, "Compound spatial sonography of the thyroid gland: evaluation of freedom from artifacts and of nodule conspicuity," AJR, Am. J. Roentgenol. **177**(5), 1195–8 (2001).
[12]S. J. Norton and M. Linzer, "Ultrasonic reflectivity tomography: reconstruction with circular transducer arrays," Ultrason. Imaging **1**(2), 154–84 (1979).
[13]P. L. Carson, C. R. Meyer, A. L. Scherzinger, T. V. Oughton, "Breast imaging in coronal planes with simultaneous pulse echo and transmission ultrasound," Science **214**, 1141–3 (1981).
[14]J. F. Greenleaf, A. Johnson, R. C. Bahn, and B. Rajagopalan, *Quantitative Cross-sectional Imaging of Ultrasound Parameters*, 1977 Ultrasonics Symposium Proc., IEEE Cat. # 77CH1264-1SU, pp. 989–995, 1977.
[15]M. P. Andre, H. S. Janee, P. J. Martin, G. P. Otto, B. A. Spivey, and D. A. Palmer, "High-speed data acquisition in a diffraction tomography system employing large-scale toroidal arrays," Int. J. Imaging Syst. Technol. **8**, 137–147 (1997).
[16]S. A. Johnson, D. T. Borup, J. W. Wiskin, F. Natterer, F. Wuebbling, Y. Zhang, C. Olsen, "*Apparatus and Method for Imaging with Wavefields using Inverse Scattering Techniques*," United States Patent No. 6,005,916 (1999).
[17]V. Z. Marmarelis, T. Kim, and R. E. Shehada, Proceedings of the SPIE: Medical Imaging 2003, San Diego, California, 23–28 Feb. 2002, Ultrasonic Imaging and Signal Processing, Paper 5035-6.
[18]D.-L. Liu, and R. C. Waag, "Propagation and backpropagation for ultrasonic wavefront design," IEEE Trans. Ultrason. Ferroelectr. Freq. Control **44**(1), 1–13 (1997).
[19]P. J. Littrup, N. Duric, S. Azevedo, D. H. Chambers, J. V. Candy, S. Johnson, G. Auner, J. Rather, and E. T. Holsapple, "Computerized ultrasound risk evaluation (CURE) system: Development of combined transmission and reflection ultrasound with new reconstruction algorithms for breast imaging," Acoust. Imaging **28**, 175–182 (2001).
[20]P. J. Littrup, N. Duric, R. R. Leach, Jr., S. G. Azevedo, J. V. Candy, T. Moore, D. H. Chambers, J. E. Mast, and E. T. Holsapple, *Characterizing Tissue with Acoustic Parameters Derived from Ultrasound Data*, Proceedings of the SPIE: Medical Imaging 2002, San Diego, California, 23–28 Feb. 2002, Ultrasound Imaging and Signal Processing, Paper 4687-43.
[21]N. Duric, P. J. Littrup, R. R. Leach, Jr., S. G. Azevedo, J. V. Candy, T. Moore, D. H. Chambers, J. Mast, and E. T. Holsapple, *Using Data Fusion to Characterize Breast Tissue*, Proceedings of the SPIE: Medical Imaging 2002, San Diego, California, 23–28 Feb. 2002, Ultrasonic Imaging and Signal Processing, Paper 4687-39.
[22]S. G. Azevedo, T. Moore, R. D. Huber, W. Ferguson, R. R. Leach, Jr., S. Benson, N. Duric, P. J. Littrup, and E. T. Holsapple, *Apparatus for Circular Tomographic Ultrasound Measurements*, Proceedings of the SPIE: Medical Imaging 2002, San Diego, California, 23–28 Feb. 2002, Ultrasonic Imaging and Signal Processing, Paper 4687-12.
[23]N. Duric, P. Littrup, E. Holsapple, A. Babkin, R. Duncan, A. Kalinin, R. Pevzner, and M. Tokarev, *Ultrasound Imaging of Breast Tissue*, Proceedings of the SPIE: Medical Imaging 2003, San Diego, California, 21–26 Feb. 2003, Ultrasonic Imaging and Signal Processing, Paper 5035-4.
[24]L. J. Huang, N. Duric, and P. Littrup, *Ultrasonic Breast Imaging Using a Wave-Equation Migration Method*, Proceedings of the SPIE: Medical Imaging 2003, San Diego, California, 21–26 Feb. 2003, Ultrasonic Imaging and Signal Processing, Paper 5035-4.
[25]N. Duric, P. J. Littrup, A. Babkin, D. Chambers, S. Azevedo, A. Kalinin, R. Pevzner, M. Tokarev, E. Holsapple, O. Rama, and R. Duncan, "Development of ultrasound tomography for breast imaging: Technical assessment," Med. Phys. **32**, 1375–1386 (2005).
[26]N. Duric, P. J. Littrup, O. Rama, and E. T. Holsapple, "Computerized ultrasound risk evaluation (CURE): First clinical results," *Acoustical Im-*

aging, edited by M. P. Andre (Springer, Dordrecht, 2006), Vol. 28, pp. 177–185.
[27]http://www.medipattern.com
[28]http://www.techniscanmedicalsystems.com/
[29]D. D. Dorney, J. L. Johnson, V. J. Rudd, R. G. Baraniuk, W. W. Symes, and D. M. Mittleman, "Terahertz reflection imaging using Kirchoff migration," Opt. Lett. **26**, 1513–1515 (2001).
[30]F. Natterer and F. Wubbeling, "Mathematical methods in image reconstruction," *Monographs on Mathematical Modeling and Computation* (Society for Industrial and Applied Mathematics, Philadelphia, USA, 2001).
[31]F. Natterer, "The mathematical of computerized tomography," *Classics in Applied Mathematics* (Society for Industrial and Applied Mathematics, Philadelphia, USA, 2001).